Optics Letters

On-axis deflectometric system for freeform surface measurement

Shengtai Zhu,[1] Daodang Wang,[1,2] Wenjun Kang,[1] and Rongguang Liang[1,3]

[1]Wyant College of Optical Sciences, University of Arizona, Tucson, Arizona 85721, USA
[2]wangdaodang@arizona.edu
[3]rliang@optics.arizona.edu

Received 20 January 2023; revised 28 February 2023; accepted 7 March 2023; posted 8 March 2023; published 3 April 2023

We propose an on-axis deflectometric system for the accurate measurement of freeform surfaces with large slope ranges. A miniature plane mirror is attached on the illumination screen to fold the optical path and achieve the on-axis deflectometric testing. Due to the existence of the miniature folding mirror, the deep-learning method is applied to recover the missing surface data in a single measurement. Low sensitivity to the calibration error of system geometry and high testing accuracy can be achieved with the proposed system. The feasibility and accuracy of the proposed system have been validated. The system is low in cost and simple in configuration, and it provides a feasible way for the flexible and general testing of freeform surfaces, with a significant potential of the application in on-machine testing.

https://doi.org/10.1364/OL.486170

Freeform optics have been widely used in high-performance optical systems as they provide additional degrees of freedom for optimization. However, due to the loss of rotational symmetry and high slope range in surface profile, it is very challenging to achieve the freeform surface testing with high accuracy and flexibility. As a non-contact and full-field metrology method, interferometry can achieve accurate surface testing of the order of subwavelength. However, it is limited in measurable dynamic range and flexibility, and additional null optics, such as a computer-generated hologram (CGH) [1], are required for the testing of surfaces with large slope ranges. Such null optics are expensive to fabricate and only work for one specific tested surface, and it is also difficult to adjust the null position, making them inflexible and unsuitable for testing the freeform surfaces with large slope ranges.

Deflectometry has been investigated as a promising approach for freeform surface testing, as it has both large slope dynamic range and simple system configuration. In 2004, Knauer, Kaminski, and Hausler proposed phase-measuring deflectometry (PMD) [2] to measure a freeform surface for the first time. Since then, PMD has been intensively studied and widely applied in many areas, such as specular surface inspection [3], deformation measurement [4], and refractive surface reconstruction [5]. A typical PMD system generally consists of a liquid crystal display (LCD) screen, a camera, and the surface under test (SUT). To retrieve the surface profile from the captured images, the system geometry needs to be well calibrated, and then the surface slope can be calculated and integrated to reconstruct the tested surface. The testing accuracy of PMD highly depends on the achievable accuracy in system geometry calibration, and additional surface measurement error (especially low-frequency surface error) could be introduced due to inaccurate calibration (geometric error) [6]. To address this issue, various methods have been proposed to minimize the effect of geometric error. One type of the method is computer-aided calibration, including the model-based PMD (MPMD) [7] and computer-aided reverse optimization [6,8]. In these methods, various merit functions are defined to optimize the system geometry parameters, and the geometrical aberrations can be effectively removed based on the calibrated geometry parameters. These methods are easy to perform, however, overcorrection may exist and could introduce residual geometrical aberrations. Another approach is to employ the on-axis system configuration, by which the testing is much less sensitive to geometric uncertainty relative to that in the traditional off-axis configuration [9]. It provides a feasible way to address the system miscalibration. In addition, the camera can capture the SUT perpendicularly, making the measurement free from perspective distortion. This configuration is also preferable in stereo deflectometry as it greatly reduces shadows caused by discontinuities in the SUT and makes the system more compact [10,11]. The existing on-axis configurations of PMD systems are built based on a beam splitter [9,11,12], which is applied to combine the two optical axes in the fringe-illumination path and imaging path. The geometry sensitivity can be significantly reduced with this configuration. However, its effective working space is limited by the dimension of the beam splitter and an additional systematic error could be inherently introduced due to the thickness and shape variation of the beam splitter. To minimize the effect of the beam splitter, a high-quality beam splitter with additional calibration is generally required, making the system setup costly and measurement process complicated.

In this Letter, a novel on-axis deflectometric system (ODS) is proposed for the accurate freeform surface measurement. Instead of using a traditional beam splitter to build the on-axis configuration, the proposed ODS uses a miniature plane mirror, which is attached on the illumination screen, to fold the optical path. Thus, the limited working space and inherent systematic error from the beam splitter can be avoided. Furthermore, a distortion-corrected imaging system is aligned on the folded optical axis to

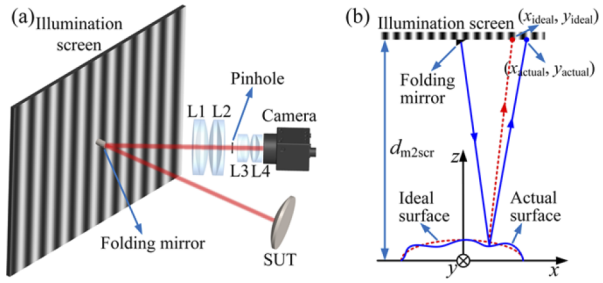

Fig. 1. Schematic of the ODS: (a) system layout and (b) measurement principle.

record the deformed pattern reflected by the SUT. Both a high measurement accuracy and large slope dynamic range can be achieved with the ODS. In addition to being much less sensitive to geometric error relative to the off-axis configuration, the ODS is low in cost and easy to operate, making it extremely promising for the accurate, flexible, and general testing of freeform surfaces.

The schematic configuration of the proposed ODS is shown in Fig. 1(a). An LCD illumination screen (INNOCN 27C1U, resolution, 3480 × 2160; pixel size, 0.1554 mm) is aligned with the optical axis of SUT and illuminates the SUT with coded sinusoidal fringe patterns. A miniature folding plane mirror M (diameter, 2 mm; flatness, 78.6 nm) is attached on the screen to fold the optical path. The reflected deformed fringe from the SUT is collected by a distortion-corrected imaging lens group consisting of four doublet lenses L1–L4 (L1 and L2, Thorlabs AC508-150-A; diameter, 2″; L3 and L4, Thorlabs AC254-050-A; diameter, 1″) and imaged on a CCD camera (PointGrey, FL3-U3-13S2M-CS; resolution, 1328 × 1048; pixel size; 3.63 μm). To reduce the distortion in the imaging, an adjustable pinhole is placed at the conjugate position of the mirror M between the lenses L2 and L3 to form a symmetrical optical system, in which the transversal aberrations before and after the stop have opposite signs. M and L1 are the entrance pupil and field aperture, respectively, and the maximum measurable surface diameter is approximately 82 mm. With a finite size of the aperture, a pinhole camera model can be used to uniquely define the mapping relationship between the incident and reflected rays on the SUT. The wavefront reconstruction principle of ODS is similar with that of a typical PMD system [13], except that our camera and SUT are aligned on-axis. Sinusoidal fringes in the x and y directions at three different frequencies are displayed on the illumination screen to illuminate the SUT. The absolute phase distribution corresponding to the distorted fringe patterns can be retrieved with a temporal phase unwrapping algorithm [14] to determine the incident and reflected rays on the SUT, from which the tested surface can be reconstructed.

The principle of the ODS can be interpreted as a reverse Hartmann test, as is shown in Fig. 1(b). The rays start from the center of mirror M, then are reflected by the SUT, and finally reach the screen plane, which results in a spot distribution (x_{actual}, y_{actual}). By building an ideal system model corresponding to the actual system configuration, the ideal spot distribution (x_{ideal}, y_{ideal}) can be obtained with ray tracing from the aperture to screen plane. The SUT surface error can be obtained with a virtual null testing. By comparing the actual and ideal spot distributions, we have the slope of the surface error according to the transverse ray aberration model [15]:

$$\begin{cases} \Delta w_x = \partial W(x,y)/\partial x \cong -\Delta x_{\text{spot}}/d_{\text{m2scr}} \\ \Delta w_y = \partial W(x,y)/\partial y \cong -\Delta y_{\text{spot}}/d_{\text{m2scr}} \end{cases}, \tag{1}$$

where d_{m2scr} is the distance between the SUT and illumination screen, $\Delta x_{\text{spot}} = x_{\text{actual}} - x_{\text{ideal}}$, $\Delta y_{\text{spot}} = y_{\text{actual}} - y_{\text{ideal}}$; $(\Delta w_x, \Delta w_y)$ are the slopes of the surface error in x and y directions, and $W(x, y)$ is the wavefront aberration. The tested surface error can be obtained by integrating the slopes $(\Delta w_x, \Delta w_y)$. The ODS provides a flexible way for accurate freeform surface testing with a large slope range.

There are three key performance parameters in the ODS, those are the slope range ξ_s, spatial resolution δ_x, and angular resolution δ_α. The slope range δ_s is determined by the illumination screen size L_{scr} and the distance d_{m2scr} between the SUT and illumination screen, and we have the slope range $\xi_s = L_{\text{src}}/2d_{\text{m2scr}}$. There is a trade-off between the spatial and angular resolutions [2], which can be expressed as $\delta_x \dot{c} \delta_\alpha = \pi\lambda/Q$, where λ is the illumination wavelength and Q is the system quality factor related to the signal-to-noise ratio (SNR). The ideal spatial resolution δ_x is given by the diffraction limitation, $\delta_r = 1.22\lambda/D$, where D is the diameter of the entrance pupil. The angular uncertainty is $\delta_\alpha = \delta_{\text{pixel}} U_{\text{phase}} / 2d_{\text{m2scr}}$ [13], where δ_{pixel} is the pixel pitch of the illumination screen and U_{phase} is the phase uncertainty. Thus, we have the slope dynamic range $\xi_s = 0.98$ rad, spatial resolution $\delta_r = 0.057$ mm, and slope resolution $\delta_a = 4.6$ μrad, corresponding to the given the phase uncertainty $U_{\text{phase}} = 0.01$ pixel, screen size $L_{\text{src}} = 335.6$ mm, screen pixel size $\delta_{\text{pixel}} = 0.1554$ mm, distance $d_{\text{m2scr}} = 170$ mm, aperture diameter $D = 2$ mm, and central illumination wavelength $\lambda = 0.55$ μm.

The calibration of the system geometry, including the positions and orientations of the SUT, illumination screen, and camera aperture, is a key issue in traditional PMD. Miscalibration of the system geometry could introduce a significant residual error in the final result. To validate the flexibility of the proposed ODS, a ray-tracing-based simulation was performed to analyze the effect of the system geometry uncertainty on the traditional off-axis PMD and the ODS, in which the SUT was a 1-inch aspheric mirror with the conic constant $K = -0.8$ and radius $R = 25$ mm. The distance between the SUT and illumination screen, and that between the SUT and camera aperture in z direction are 170 mm and 165 mm, respectively, and the off-axis distance h of the camera varies from 0 to 150 mm (corresponding to the change from on-axis configuration to off-axis configuration with various off-axis distances). Without loss of generality, the camera is set to be off-axis in the x direction. The lateral displacement uncertainty of the camera in the x and y directions are both 0.1 mm, and the tilt angle uncertainty of the illumination screen about the x and y axes are both 0.05 degrees. The wavefront error introduced by the geometry uncertainty could be represented with Zernike polynomials $\{Z_i\}$. Figure 2 shows the low-order aberrations introduced by various geometric errors under different off-axis distances, where the Zernike terms Z_5–Z_{11} refer to astigmatism x and y, coma x and y, trefoil x and y, and primary spherical aberration, respectively. It can be seen from Fig. 2 that, as the system departures from the on-axis configuration, the low-order aberrations, especially astigmatism and coma, grow significantly with off-axis distance of the camera. For the off-axis configuration with 150-mm off-axis distance of camera, the 0.05° tilt error about the y axis would introduce 0.43-μm astigmatism, 0.20-μm coma, 0.09-μm trefoil, and 0.05-μm primary spherical aberrations, respectively; however, there

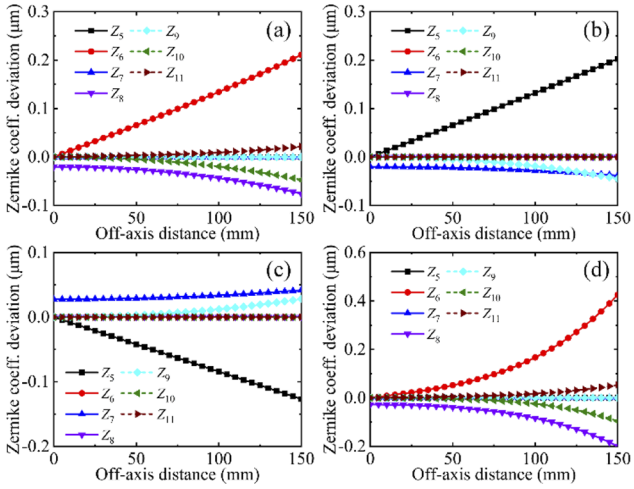

Fig. 2. Sensitivity to geometric uncertainties of PMD. Aberrations induced by 0.1-mm camera position uncertainty in (a) x and (b) y directions, and those induced by 0.05° screen tilt uncertainty about the (c) x and (d) y axes.

are only 0.06-nm astigmatism, 28-nm coma, 0.02-nm trefoil, and 0.003-nm primary spherical aberrations in the on-axis configuration with the same angle of uncertainty. In the case of the ODS with an on-axis configuration, all the low-order aberrations, except for coma (which is very small compared to that of the off-axis configuration), induced by various geometric uncertainties are restricted to near zero. Therefore, the on-axis configuration design makes the ODS much less sensitive to geometric errors, where the low-order aberrations, especially astigmatism due to geometry miscalibration, can be well restricted.

To demonstrate the feasibility and high accuracy of the ODS, an aspheric mirror with the conic constant $K = -0.8$ and radius $R = 25$ mm was measured with the system. The distance d_{m2scr} between the SUT and illumination screen is approximately 170 mm, and the working distance of the camera is 165 mm. The system geometry was calibrated using a coordinate measuring machine (TESA micro-hite 3D; accuracy, 7.0 μm), and the imaging system was calibrated with Zhang's method [16]. Figure 3(a) shows the surface map measured with the ODS, with the peak-to-valley (PV) and root mean square (rms) values of 2.3135 μm and 0.6361 μm, respectively. For comparison, the tested surface has also been measured with a Zygo Verifire interferometer, and the obtained surface map is shown in Fig. 3(d), with the PV and rms values of 2.1933 μm and 0.6299 μm. To verify the low sensitivity of the ODS to the calibration error of the system geometry and its flexibility in practical application, an additional geometrical error (AGE), including with a 10-μm lateral displacement error of camera and a 0.05° tilt error of illumination screen about the y axis, was added in the ray-tracing model, with the obtained surface map being shown in Fig. 3(b). To

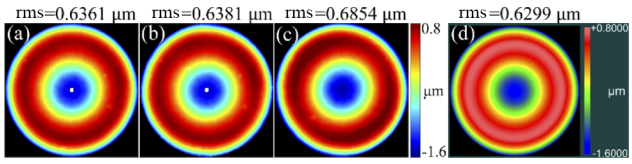

Fig. 3. Measured surface maps of an aspheric surface: (a) proposed ODS; (b) ODS with AGE; (c) off-axis configuration; and (d) Zygo interferometer.

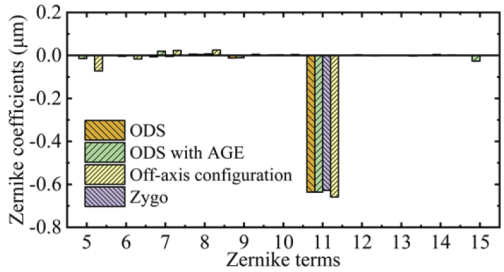

Fig. 4. Comparison of Zernike coefficients in the testing of an aspheric mirror.

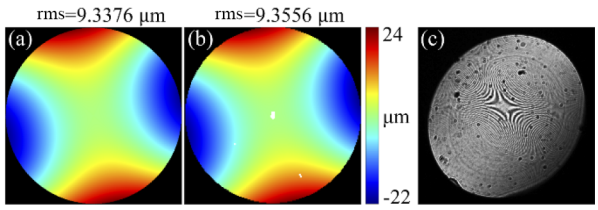

Fig. 5. Measurement results of a freeform surface. (a) Nominal surface. (b) Measured surfaces with the ODS. (c) Interferogram acquired with Zygo interferometer.

further show the advantage of the ODS over the off-axis configuration, the SUT was shifted in the x direction for 100 mm, and additional measurement with the re-calibrated off-axis system was performed, with the measurement result being shown in Fig. 3(c) (PV = 2.7598 μm, rms = 0.6854 μm). Figure 4 presents the comparison of the Zernike coefficients (Z_5–Z_{15}) of the measured surface maps in Fig. 3. From Figs. 3 and 4, we can clearly see that the measurement result obtained with the ODS agrees well with that of the Zygo interferometer, and the difference in rms value is 0.0062 μm, indicating the feasibility and high accuracy of the proposed ODS. The geometrical aberration in the ODS is much less than that of the off-axis configuration. In addition, even though an additional calibration error is added, the change in the reconstructed surface is only of the order of nanometers, demonstrating the low sensitivity of ODS to geometric errors. It should be noted that a minor deviation from the Zygo result in the low-order Zernike coefficients can be seen in Fig. 4, and it is mainly caused by the slight system misalignment.

To further validate the feasibility of the ODS for the freeform surface testing with a large slope range, a diamond-turning freeform surface with the conic constants $K_x = -2$ and $K_y = -1$, radius $R_x = 23.5$ mm and $R_y = 26.5$ mm was measured. Figure 5(a) shows the nominal surface map of the tested freeform surface, whose PV and rms values are 44.2481 μm and 9.3376 μm, respectively. The slope range of the tested freeform surface is 0.2152 rad, and it exceeds the measurable range of a conventional laser interferometer [with the acquired interferogram being shown in Fig. 5(c)]. Figure 5(b) shows the surface map measured with the ODS, with the PV and rms values of 45.0240 μm and 9.3556 μm, respectively. The comparison of the Zernike coefficients for the nominal surface map and the surface measured with the ODS is given in Fig. 6. According to Figs. 5 and 6, a good agreement between the nominal surface and the measured one with ODS are achieved, with the rms difference being 0.0180 μm. Therefore, the proposed ODS provides a feasible way for the flexible testing of freeform surfaces.

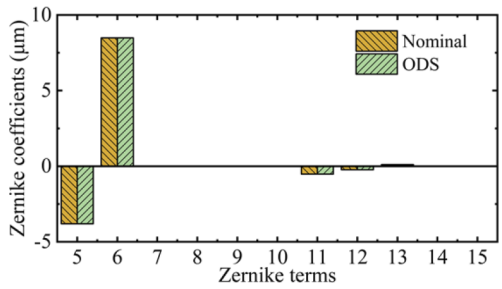

Fig. 6. Comparison of Zernike coefficients in the testing of a freeform surface.

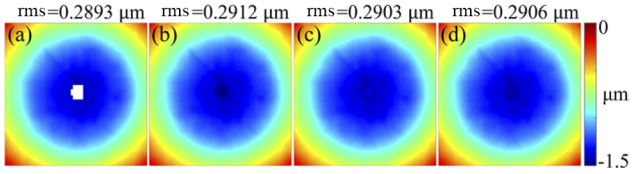

Fig. 7. Missing data recovery in the measured surface maps. (a) Surface map with missing data. Recovered surface maps with (b) spline interpolation, (c) stitching method, and (d) D-UNet.

The folding mirror M could introduce a measurement error due to its imperfect surface shape. According to the ray-tracing results, the rms of the introduced wavefront error from the flatness of the mirror M is 1.24 nm, which is negligible. Due to the existence of the folding mirror M attached on the illumination screen, partial sampling rays from the screen to the SUT would be blocked, resulting in the missing data in the central region of the SUT [Figs. 3(a) and 5(b)]. Various solutions can be adopted to address this issue, including the interpolation, stitching technique, and deep-learning method. Interpolation (such as spline interpolation) is a direct and simple approach to filling the missing data; however, it fails in the case of a large missing region. The stitching method requires an additional measurement to acquire the missing surface data by laterally shifting the SUT. As an efficient tool in image inpainting [17], the deep-learning method provides a flexible approach to addressing the partially missing data in the measurement, even feasible in the case of a large missing region. The D-UNet network [18] can be applied to retrieve the missing data due to the existence of the folding mirror M in the ODS. This network uses full-scale skip connections to extract multi-scale features to achieve both high accuracy and robustness. A dataset of 10,000 normalized surface maps with missing data and additional Gaussian noise were randomly generated, in which 8000 figures were used to train the network and the other 2000 figures were assigned to the test dataset. The rms of the difference between the prediction and ground truth is set as the loss function to train the network, and the final test loss is 6×10^{-4}, indicating that the trained D-UNet is high in accuracy and robust to noise. Figure 7(a) shows the original surface map (PV = 1.3615 μm, rms = 0.2893 μm) with missing data in the central 10% region of Fig. 3(a), and Figs. 7(b)–7(d) are the surface maps with the missing data recovered with the spline interpolation (PV = 1.4159 μm, rms = 0.2912 μm), stitching method (PV = 1.3615 μm, rms = 0.2903 μm), and D-UNet algorithm (PV = 1.3615 μm, rms = 0.2906 μm), respectively. From Fig. 7, a better agreement between the recovered surfaces with the D-UNet algorithm and the stitching method (with the result taken as the ground truth) can be observed relative to that of interpolation, validating the reliability and flexibility of the D-UNet algorithm for missing data recovery with a single measurement in the ODS.

In conclusion, the proposed ODS provides an accurate, flexible, and general way for the testing of freeform surfaces with large slope dynamic ranges. Due to its on-axis configuration, the proposed system is much less sensitive to system geometric error than the traditional off-axis PMD. In addition, the use of a miniature folding mirror avoids the limitation in working space and inherent systematic error in the existing beam splitter-based on-axis PMD, making the system low in cost and simple in configuration. Both the high accuracy and large slope dynamic range have been verified. It provides a powerful tool for the flexible and general testing of freeform surfaces, with a significant potential of the application in on-machine testing.

Funding. National Science Foundation (1918260, 2034210); National Institutes of Health (S10OD018061).

Disclosures. The authors declare no conflicts of interest.

Data availability. Data underlying the results presented in this Letter are not publicly available at this time but may be obtained from the authors upon reasonable request.

REFERENCE

1. C. Pruss, S. Reichelt, H. J. Tiziani, and W. Osten, Opt. Eng. **43**, 2534 (2004).
2. M. C. Knauer, J. Kaminski, and G. Hausler, Proc. SPIE **5457**, 366 (2004).
3. S. Werling, M. Mai, M. Heizmann, and J. Beyerer, Metrol. Meas. Syst. **16**, 415 (2009).
4. L. Huang, C. S. Ng, and A. K. Asundi, Opt. Lasers Eng. **50**, 529 (2012).
5. D. Wang, P. Xu, Z. Wu, X. Fu, R. Wu, M. Kong, J. Liang, B. Zhang, and R. Liang, Optica **7**, 1056 (2020).
6. D. Wang, S. Zhang, R. Wu, C. Y. Huang, H.-N. Cheng, and R. Liang, Opt. Express **24**, 19671 (2016).
7. L. Huang, J. Xue, B. Gao, C. McPherson, J. Beverage, and M. Idir, Opt. Express **24**, 24649 (2016).
8. D. Wang, Z. Gong, P. Xu, C. Wang, R. Liang, M. Kong, and J. Zhao, Opt. Express **26**, 8113 (2018).
9. R. Huang, P. Su, T. Horne, G. Brusa, and J. H. Burge, Opt. Eng. **53**, 085106 (2014).
10. F. Gao, Y. Xu, and X. Jiang, Opt. Lasers Eng. **158**, 107195 (2022).
11. F. Gao, Y. Xu, and X. Jiang, Opt. Express **30**, 17554 (2022).
12. Z. Gu, D. Wang, Y. Ruan, M. Kong, X. Xu, and R. Liang, Appl. Opt. **61**, 2856 (2022).
13. P. Su, R. E. Parks, L. Wang, R. P. Angel, and J. H. Burge, Appl. Opt. **49**, 4404 (2010).
14. S. Zhang, Opt. Lasers Eng. **107**, 28 (2018).
15. J. Rayces, Opt. Acta **11**, 85 (1964).
16. Z. Zhang, IEEE Trans. Pattern Anal. Machine Intell. **22**, 1330 (2000).
17. Z. Qin, Q. Zeng, Y. Zong, and F. Xu, Displays **69**, 102028 (2021).
18. J. Dou, D. Wang, Q. Yu, M. Kong, L. Liu, X. Xu, and R. Liang, Opt. Lett. **47**, 78 (2022).